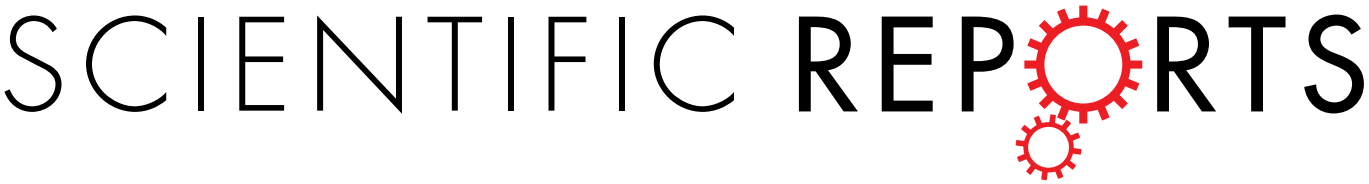

OPEN

Single-electron Spin Resonance in a Quadruple Quantum Dot

Tomohiro Otsuka[1,2], Takashi Nakajima[1,2], Matthieu R. Delbecq[1,2], Shinichi Amaha[1], Jun Yoneda[1,2], Kenta Takeda[1,2], Giles Allison[1], Takumi Ito[1,2], Retsu Sugawara[1,2], Akito Noiri[1,2], Arne Ludwig[3], Andreas D. Wieck[3] & Seigo Tarucha[1,2,4,5]

Received: 19 May 2016
Accepted: 21 July 2016
Published: 23 August 2016

Electron spins in semiconductor quantum dots are good candidates of quantum bits for quantum information processing. Basic operations of the qubit have been realized in recent years: initialization, manipulation of single spins, two qubit entanglement operations, and readout. Now it becomes crucial to demonstrate scalability of this architecture by conducting spin operations on a scaled up system. Here, we demonstrate single-electron spin resonance in a quadruple quantum dot. A few-electron quadruple quantum dot is formed within a magnetic field gradient created by a micro-magnet. We oscillate the wave functions of the electrons in the quantum dots by applying microwave voltages and this induces electron spin resonance. The resonance energies of the four quantum dots are slightly different because of the stray field created by the micro-magnet and therefore frequency-resolved addressable control of each electron spin resonance is possible.

Electron spins in semiconductor quantum dots (QDs) have relatively long coherence times in solid state devices[1–4] and potential scalability by utilizing current extensive semiconductor fabrication techniques. Considered good candidates for quantum bits[5] in quantum information processing[6,7], the required elementary operations on the spin-1/2 qubits for quantum information processing have been demonstrated recently. The spin states are initialized and read out using the Pauli spin blockade (PSB)[8] or tunneling to the leads from Zeeman split energy levels[9,10]. Rotation of single spins has been realized by electron spin resonance (ESR)[11]. Addressability and the speed of single spin rotation are improved by micro-magnet (MM) induced ESR[12,13]. High-fidelity single-spin rotation decoupled from the fluctuating nuclear spin environment was demonstrated[14]. Entanglement operations of two spins are realized by utilizing exchange interaction and fast two qubit operations have been demonstrated[15–18]. This scheme for the spin-1/2 qubit is applicable to a wide variety of materials including Si, which has a long spin coherence time[3,4].

Scale up of the QD system is crucial to realize larger scale quantum gate operations and also explore multi-spin physics. To this end, spin qubit experiments on multiple QDs have been reported in recent years. In triple QDs, PSB has been observed[19,20] and the exchange only qubit utilizing a triple QD as a single qubit has been demonstrated[21–24]. Towards three spin-1/2 qubits[25], ESR in a triple QD was recently realized[26]. Experiments on quadruple QDs (QQDs) have also been started[27,28], and a QQD is utilized for realization of two qubit operations on singlet-triplet qubits[29]. For four spin-1/2 qubits, the precise charge state control in a tunnel coupled QQD has been demonstrated in the few-electron regime[30].

In this paper, we demonstrate four distinctly addressable electron spin resonances in a QQD. First, we realize few-electron charge states in a QQD required to observe PSB. Second, we observe PSB for readout of ESR signals. The blocked triplet components are created by singlet-triplet mixing induced by the nuclear spins and the MM. Finally, we observe four ESR signals corresponding to the four individual spins in the QQD.

Results

Device and Charge states. Figure 1(a) shows a scanning electron micrograph of the device. By applying negative voltages on the gate electrodes, which appear light gray in the picture, a QQD and two QD charge sensors[31] are formed at the lower and the upper sides, respectively. The QD charge sensors are connected to

[1]Center for Emergent Matter Science, RIKEN, 2-1 Hirosawa, Wako, Saitama 351-0198, Japan. [2]Department of Applied Physics, University of Tokyo, Bunkyo, Tokyo 113-8656, Japan. [3]Angewandte Festkörperphysik, Ruhr-Universität Bochum, D-44780 Bochum, Germany. [4]Quantum-Phase Electronics Center, University of Tokyo, Bunkyo, Tokyo 113-8656, Japan. [5]Institute for Nano Quantum Information Electronics, University of Tokyo, 4-6-1 Komaba, Meguro, Tokyo 153-8505, Japan. Correspondence and requests for materials should be addressed to T.O. (email: tomohiro.otsuka@riken.jp)

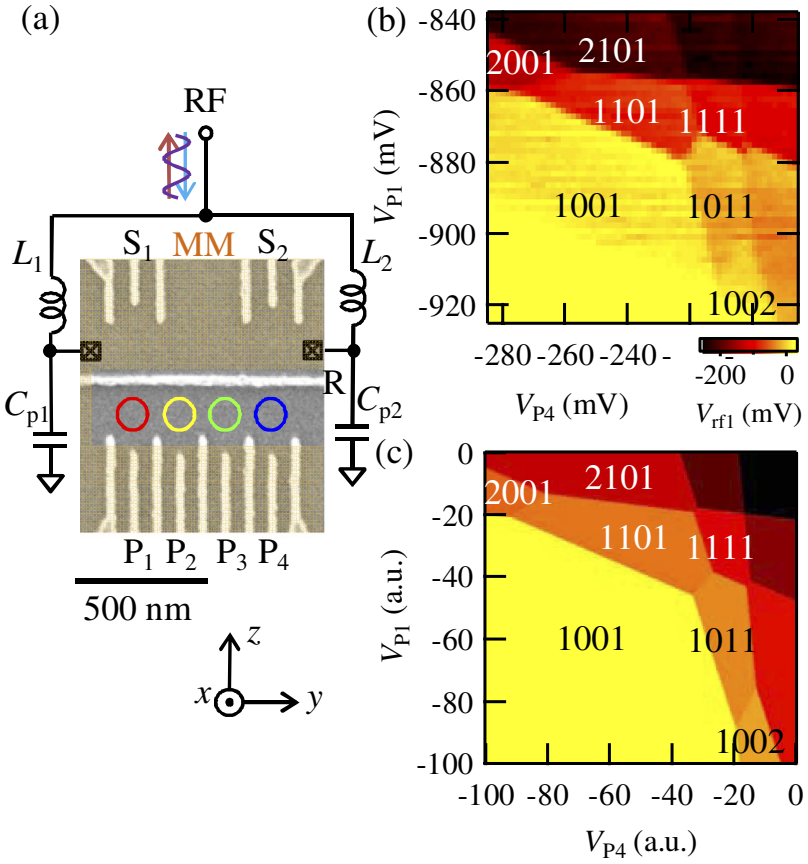

Figure 1. (**a**) Scanning electron micrograph of the device and the schematic of the measurement setup. A QQD is formed at the lower side and the charge states are probed by the charge sensor QDs at the upper side. The charge sensors are connected to resonators formed by the inductors L_1 and L_2 and the stray capacitances C_{p1} and C_{p2} for the RF reflectometry. A MM is deposited on the shaded region on the top of the device, which creates local magnetic fields to induce ESR. The external magnetic field is applied in plane along the z axis. (**b**) V_{rf1} as a function of V_{P4} and V_{P1}. Changes of the charge states are observed. The number of the electrons in each QD is shown as n_1, n_2, n_3, n_4. (**c**) Calculated charge stability diagram of a QQD. The experimental result (**b**) is reproduced by considering the capacitively coupled QQD model. n_1, n_2, n_3, n_4 are shown in the figure.

RF resonators formed by the inductors L_1 and L_2 and the stray capacitances C_{p1} and C_{p2} (resonance frequency $f_{res1} = 298$ MHz, $f_{res2} = 207$ MHz) for the RF reflectometry[31–33]. The number of electrons in each QD n_1, n_2, n_3, and n_4 is monitored by the intensity of the reflected RF signal V_{rf1} and V_{rf2}. A change in the electrostatic environment around the sensing dots changes their conductance, shifts the tank circuit resonance and modifies V_{rf1} and V_{rf2} measured at f_{res1} and f_{res2}. A MM is deposited on the shaded region on the top of the device, which creates local magnetic fields to induce ESR. The external magnetic field is applied in the plane along the z axis to induce Zeeman splitting and magnetizes the MM. The shape of the MM is specially designed to realize strong driving of the electron spin rotations by the large field gradient and splitting of the ESR frequencies by the Zeeman field differences between the dots[34]. Thanks to this MM, we can realize a stable magnetic field which is difficult to achieve by the fluctuating nuclear spins and the scheme is material independent.

Figure 1(b) is the charge stability diagram of the QQD. We measured V_{rf1} as a function of the plunger gate voltages of QD_4 V_{P4} and QD_1 V_{P1}. We observe the change of V_{rf1}, as the result of the charge states in the QQD. Charge transition lines with four different slopes are observed reflecting the different electrostatic coupling of the QQD to V_{P4} and V_{P1}. n_1, n_2, n_3, and n_4 are assigned as shown in Fig. 1(b) by counting the number of charge transition lines from the fully depleted condition $[n_1, n_2, n_3, n_4] = [0, 0, 0, 0]$. Figure 1(c) shows the calculated charge state of the QQD. By considering the capacitively coupled QQD model[30,35], we reproduce the observed charge stability diagram. We find the characteristic "goggle" structure, which is formed by the charge transition lines around [1, 1, 1, 1], [1, 1, 0, 1] and [1, 0, 1, 1] charge states. In the [1, 1, 1, 1] state, each dot contains a single electron and this state is useable as a four qubit system of the spin-1/2 qubit.

Spin blockade. To readout the spin states of the qubits, PSB[8] is a powerful tool. If the triplet spin states are formed in the neighboring QDs, the charge transition $[1, 1, 0, 1] \rightarrow [2, 0, 0, 1]$ ($[1, 0, 1, 1] \rightarrow [1, 0, 0, 2]$) is forbidden because of Pauli exclusion principle. In the stability diagrams in Fig. 1(b,c), the spin blockade can be expected around the charge transition lines between [1, 1, 0, 1] and [2, 0, 0, 1], and between [1, 0, 1, 1] and [1, 0, 0, 2]. Note that charge boundaries between $[1, 1, 1, 1] \rightarrow [2, 0, 1, 1]$ and $[1, 1, 1, 1] \rightarrow [1, 1, 0, 2]$, which is required to observe

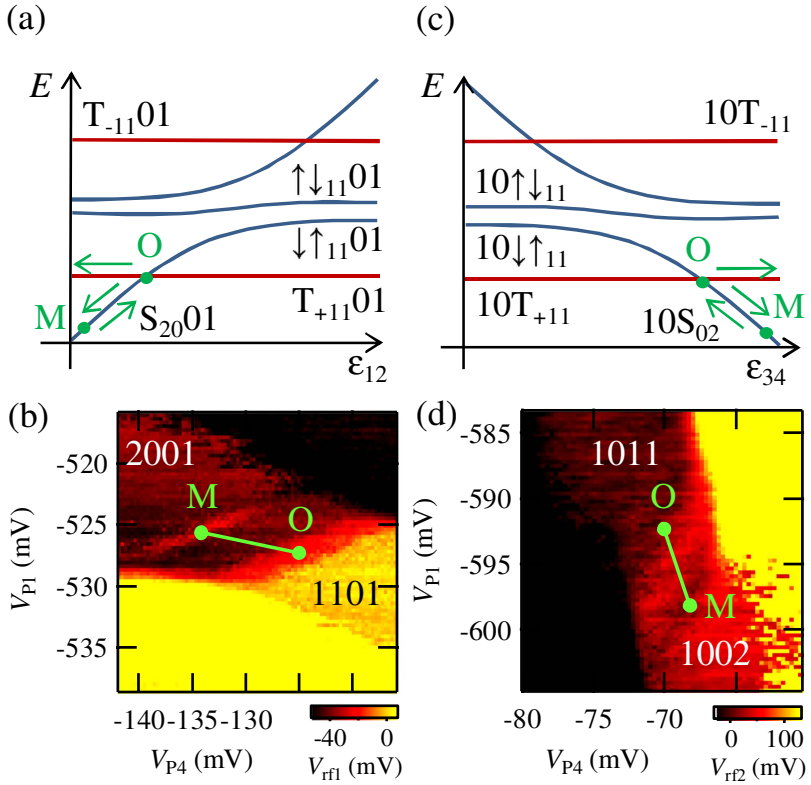

Figure 2. (**a,c**) Energy diagrams and schematics of the pulse operation to observe PSB in QD1 and QD2 (QD3 and QD4). The $T_{+11}01$ ($10T_{+11}$) component is populated at the operation point O by using the $S_{11}01 \Leftrightarrow T_{+11}01$ ($10S_{11} \Leftrightarrow 10T_{+11}$) mixing. The triplet component is observed as the [1, 1, 0, 1] ([1, 0, 1, 1]) charge state at the measurement point M. (**b**,**d**) Observed V_{rf1} (V_{rf2}) as a function of V_{P4} and V_{P1}. The pulse sequences are indicated by lines in the figures. The change of V_{rf1} (V_{rf2}) as the result of the spin blocked signals are observed around M.

PSB around the [1, 1, 1, 1] state, never coexist on a single $V_{P1} - V_{P4}$ plane and we need to switch into $V_{P1} - V_{P2}$ and $V_{P3} - V_{P4}$ planes[30]. For experimental simplicity, we choose [1, 1, 0, 1] → [2, 0, 0, 1] and [1, 0, 1, 1] → [1, 0, 0, 2] boundaries to demonstrate PSB in this work.

We apply voltage pulses on V_{P1} and V_{P4} to observe spin blocked states. The operation schematics are shown in Fig. 2(a,c). We apply an external magnetic field of 0.5 T to induce Zeeman splitting. We start from the ground singlet state in QD_1 $S_{20}01$ (in QD_4 $10S_{02}$). The triplet plus component $T_{+11}01$ in QD_1 and QD_2 ($10T_{+11}$ in QD_3 and QD_4) is populated at the operation point O by using the singlet-triplet mixing $S_{11}01 \Leftrightarrow T_{+11}01$ ($10S_{11} \Leftrightarrow 10T_{+11}$) induced by the nuclear spins and the MM stray magnetic fields[36]. At the measurement point M, the triplet components stay in the [1, 1, 0, 1] ([1, 0, 1, 1]) charge state because of PSB and the singlet components relax to the [2, 0, 0, 1] ([1, 0, 0, 2]) charge state. Then, this blockade can be observed as the change of V_{rf1} (V_{rf2}).

Figure 2(b,d) show the observed V_{rf1} (V_{rf2}) as a function of V_{P4} and V_{P1}. The operation pulses are cycled constantly at each point of the graph. We apply voltage pulses with fixed amplitudes as shown as lines in Fig. 2(b,d). The directions of the pulses on the stability diagrams are chosen to modulate the detuning, the energy difference of the levels between QD_1 and QD_2 (between QD_3 and QD_4). Note that we are also able to control QD_2 and QD_3 by V_{P1} and V_{P4} because of the finite capacitive coupling. Sensor 1 is used for Fig. 2(b) (Sensor 2 for Fig. 2(d)) to maximize the charge sensitivity. The changes of V_{rf1} (V_{rf2}) are observed around M when the operation point O hits the singlet-triplet mixing point. These correspond to the spin blocked signals.

Electron spin resonance. Next, we apply a microwave voltage on gate R to induce ESR (with the frequency f_{ESR}). The operation schematics are shown in Fig. 3(a,c). In the present device, the Zeeman field difference ΔB_z between QD_1 and QD_2 (QD_3 and QD_4) by the MM will be larger than the singlet-triplet splitting at the operation point O and the eigenstates are $\downarrow\uparrow_{11}01$ and $\uparrow\downarrow_{11}01$ ($10\downarrow\uparrow_{11}$ and $10\uparrow\downarrow_{11}$), not $S_{11}01$ and $T_{0\,11}01$ ($10S_{11}$ and $10T_{0\,11}$) (see Supplementary Information). We prepare the states $\downarrow\uparrow_{11}01$ in QD_1 and QD_2 ($10\downarrow\uparrow_{11}$ in QD_3 and QD_4) by adiabatically pulsing from $S_{20}01$ ($10S_{02}$). Then, we apply microwaves at the operation point O. These applied microwaves create an oscillating electric field around the gate R and thus induce movements of the QD electron's wave functions. These oscillations of the wave functions are converted into oscillating magnetic fields along the x axis perpendicular to the external magnetic field in the field gradient created by the MM and ESR is induced[12,13]. The triplet components $T_{+11}01$ or $T_{-11}01$ ($10T_{+11}$ or $10T_{-11}$) are populated by ESR and detected as the [1, 1, 0, 1] ([1, 0, 1, 1]) charge states.

Figure 3(b,d) show the singlet return probability P_S as a function of f_{ESR} and the external magnetic field B_{ext}. P_S is calculated from V_{rf1} (V_{rf2}) by using the method reported in the refs 23,37. The measurement time is 30 μs

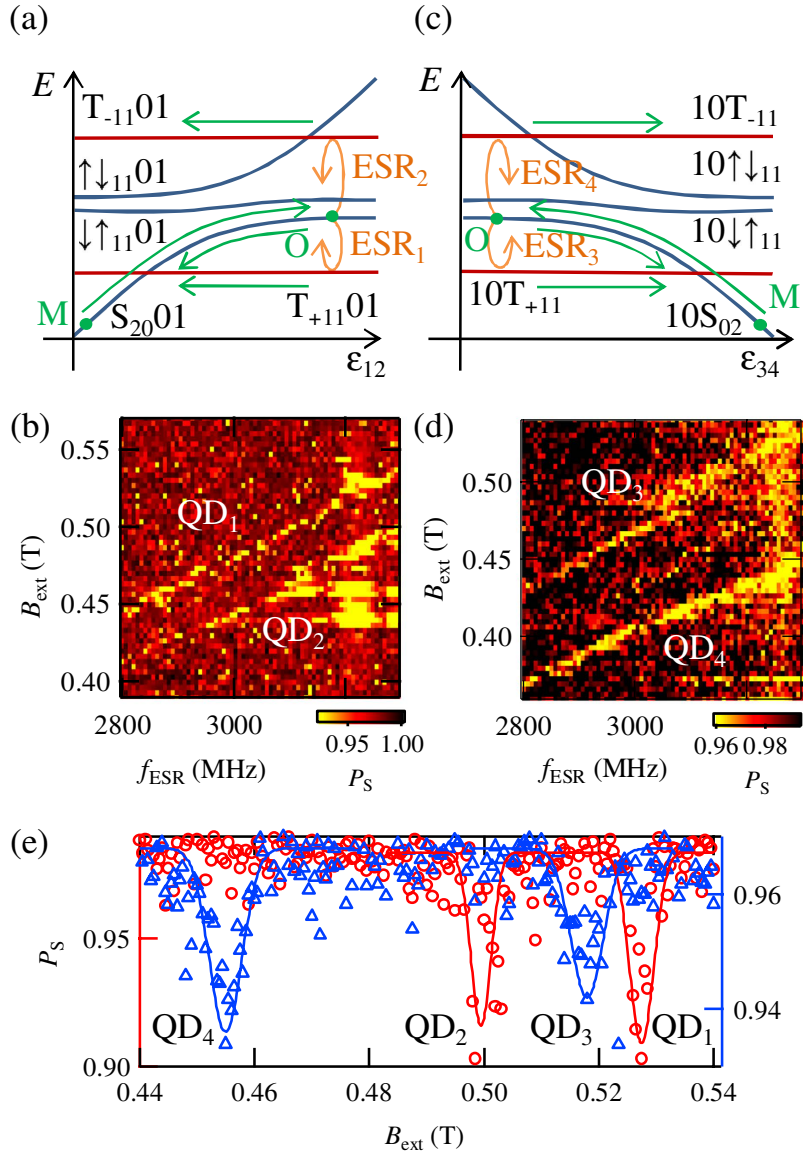

Figure 3. (**a,c**) Schematics of the energy diagrams and the pulse operations to observe ESR in QD1 and QD2 (QD3 and QD4). States are prepared as $\downarrow\uparrow_{11}01$ ($10\downarrow\uparrow_{11}$) due to ΔB_z between QD_1 and QD_2 (QD_3 and QD_4) by the MM, which is larger than the singlet-triplet splitting at the operation point O. The states evolve into $T_{+11}01$ or $T_{-11}01$ ($10T_{+11}$ or $10T_{-11}$) states by ESR. The created triplet components are observed as [1, 1, 0, 1] ([1, 0, 1, 1]) charge states at the measurement point M. (**b,d**) Observed P_S as a function of f_{ESR} and B_{ext}. ESR occurs when the applied microwave frequency matches the external magnetic field plus the stray field created by the micromagnet $hf_{ESR} = g\mu(B_{ext} + B_{MMz})$. (**e**) Observed P_S as a function of B_{ext} at $f_{ESR} = 3265$ MHz. Dips of P_S are observed when ESR occurs. The circles (triangles) show the results measured in QD1 and QD2 (QD3 and QD4). The traces are Gaussian eye guides.

and set shorter than the relaxation time $T_1 > 100$ μs. We can see the decrease of P_S when the applied microwave frequency matches the external magnetic field plus the z component of the stray field created by the MM $hf_{ESR} = g\mu(B_{ext} + B_{MMz})$. The ESR dips of P_S are also observed in Fig. 3(e), which show P_S as a function of B_{ext} at $f_{ESR} = 3265$ MHz.

Discussion

The slopes of the ESR lines in Fig. 3(b,d) give a value of the g-factor as $|g| = 0.37 \pm 0.03$ that is consistent with reported values in previous experiments[38–40].

We realize addressable control of the operation by choosing appropriate B_{ext} and f_{ESR} such that the separation of the ESR dips is larger than their width as in Fig. 3(e). From Fig. 3(e), the local Zeeman field differences between the quantum dots B_{MMz12}, B_{MMz13}, B_{MMz14} are evaluated as $B_{MMz12} = 28$ mT, $B_{MMz13} = 9$ mT, $B_{MMz14} = 73$ mT. If there is no misalignment of the QD positions, $B_{MMz12} < B_{MMz13} < B_{MMz14}$ is expected from the design of the MM[34]. This discrepancy is attributed to the misalignment of the QD positions from the center of the MM. The observed

values of the local Zeeman field are explained by shifts of the QD positions of around 100 nm in the z direction, which is possible in this QQD device (see Supplementary Information). The unexpected position-shift might be compensated by additional tuning of the gate voltages or removing inhomogeneous potentials by using undoped device structures[41–43].

In conclusion, we have demonstrated formation of few-electron charge states, and observed spin blockade and four distinct ESR signals in a QQD. The four observed ESR dips are well separated and we are able to individually address spins by choosing the appropriate B_{ext} and f_{ESR}. These results will be important for four or more spin-1/2 qubits, multiple qubit operations, and demonstration of larger scale quantum gate operations. These also contribute to exploring multi-spin physics in controlled artificial systems.

Methods

Device structure and measurement. The device was fabricated from a GaAs/AlGaAs heterostructure wafer with an electron sheet carrier density of $2.0 \times 10^{15}\,m^{-2}$ and a mobility of $110\,m^2/Vs$ at 4.2 K, measured by Hall-effect in the van der Pauw geometry. The two-dimensional electron gas is formed 90 nm under the wafer surface. We patterned a mesa by wet-etching and formed Ti/Au Schottky surface gates by metal deposition, which appear light gray in Fig. 1(a). All measurements were conducted in a dilution fridge cryostat at a temperature of 13 mK.

References

1. Bluhm, H. *et al.* Dephasing time of GaAs electron-spin qubits coupled to a nuclear bath exceeding 200 μs. *Nat. Phys*. **7,** 109–113 (2011).
2. Shulman, M. D. *et al.* Suppressing qubit dephasing using real-time Hamiltonian estimation. *Nat. Commun.* **5,** 5156 (2014).
3. Kawakami, E. *et al.* Electrical control of a long-lived spin qubit in a Si/SiGe quantum dot. *Nat. Nano*. **9,** 666–670 (2014).
4. Veldhorst, M. *et al.* An addressable quantum dot qubit with fault-tolerant control-fidelity. *Nat. Nano*. **9,** 981–985 (2014).
5. Loss, D. & DiVincenzo, D. P. Quantum computation with quantum dots. *Phys. Rev. A* **57,** 120–126 (1998).
6. Nielsen, M. A. & Chuang, I. L. *Quantum Computation and Quantum Information*. (Cambridge University Press, 2000).
7. Ladd, T. D. *et al.* Quantum computers. *Nature* **464,** 45–53 (2010).
8. Ono, K. *et al.* Current Rectification by Pauli Exclusion in a Weakly Coupled Double Quantum Dot System. *Science* **297,** 1313–1317 (2002).
9. Elzerman, J. M. *et al.* Single-shot read-out of an individual electron spin in a quantum dot. *Nature* **430,** 431–435 (2004).
10. Nowack, K. C. *et al.* Single-Shot Correlations and Two-Qubit Gate of Solid-State Spins. *Science* **333,** 1269–1272 (2011).
11. Koppens, F. H. L. *et al.* Driven coherent oscillations of a single electron spin in a quantum dot. *Nature* **442,** 766–771 (2006).
12. Tokura, Y. *et al.* Coherent Single Electron Spin Control in a Slanting Zeeman Field. *Phys. Rev. Lett.* **96,** 047202 (2006).
13. Pioro-Ladriere, M. *et al.* Electrically driven single-electron spin resonance in a slanting Zeeman field. *Nat. Phys*. **4,** 776–779 (2008).
14. Yoneda, J. *et al.* Fast Electrical Control of Single Electron Spins in Quantum Dots with Vanishing Influence from Nuclear Spins. *Phys. Rev. Lett.* **113,** 267601 (2014).
15. Petta, J. R. *et al.* Coherent Manipulation of Coupled Electron Spins in Semiconductor Quantum Dots. *Science* **309,** 2180–2184 (2005).
16. Brunner, R. *et al.* Two-Qubit Gate of Combined Single-Spin Rotation and Interdot Spin Exchange in a Double Quantum Dot. *Phys. Rev. Lett.* **107,** 146801 (2011).
17. Maune, B. M. *et al.* Coherent singlet-triplet oscillations in a silicon-based double quantum dot *Nature* **481,** 344–347 (2012).
18. Veldhorst, M. *et al.* A two-qubit logic gate in silicon *Nature* **526,** 410–414 (2015).
19. Kobayashi, T. *et al.* Cooperative Lifting of Spin Blockade in a Three-Terminal Triple Quantum Dot. arXiv:1311.6582 (2013).
20. Amaha, S. *et al.* Two- and Three-Electron Pauli Spin Blockade in Series-Coupled Triple Quantum Dots. *Phys. Rev. Lett.* **110,** 016803 (2013).
21. Laird, E. A. *et al.* Coherent spin manipulation in an exchange-only qubit *Phys. Rev. B* **82,** 075403 (2010).
22. Gaudreau, L. *et al.* Coherent control of three-spin states in a triple quantum dot *Nature Physics* **8,** 54–58 (2012).
23. Medford, J. *et al.* Self-consistent measurement and state tomography of an exchange-only spin qubit *Nature Nanotech* **8,** 654–659 (2013).
24. Eng, K. *et al. Science Advances.* **1,** e1500214 (2015).
25. Takakura, T. *et al.* Triple quantum dot device designed for three spin qubits *Appl. Phys. Lett.* **97,** 212104 (2010).
26. Noiri, A. *et al.* Coherent electron-spin-resonance manipulation of three individual spins in a triple quantum dot. *Appl. Phys. Lett* **108,** 153101 (2016).
27. Thalineau, R. *et al.* A few-electron quadruple quantum dot in a closed loop. *Appl. Phys. Lett.* **101,** 103102 (2012).
28. Takakura, T. *et al.* Single to quadruple quantum dots with tunable tunnel couplings. *Appl. Phys. Lett.* **104,** 113109 (2014).
29. Shulman, M. D. *et al.* Demonstration of Entanglement of Electrostatically Coupled Singlet-Triplet Qubits *Science* **336,** 202–205 (2012).
30. Delbecq, M. R. *et al.* Full control of quadruple quantum dot circuit charge states in the single electron regime. *Appl. Phys. Lett.* **104,** 183111 (2014).
31. Barthel, C. *et al.* Fast sensing of double-dot charge arrangement and spin state with a radio-frequency sensor quantum dot. *Phys. Rev. B* **81,** 161308 (2010).
32. Schoelkopf, R. J. *et al.* The Radio-Frequency Single-Electron Transistor (RF-SET): A Fast and Ultrasensitive Electrometer. *Science* **280,** 1238–1242 (1998).
33. Reilly, D. J., Marcus, C. M., Hanson, M. P. & Gossard, A. C. Fast single-charge sensing with a rf quantum point contact. *Appl. Phys. Lett.* **91,** 162101 (2007).
34. Yoneda, J. *et al.* Robust micromagnet design for fast electrical manipulations of single spins in quantum dots. *Appl. Phys. Exp*. **8,** 084401 (2015).
35. van der Wiel, W. G. *et al.* Electron transport through double quantum dots. *Rev. Mod. Phys*. **75,** 1–22 (2002).
36. Chesi, S. *et al.* Single-spin manipulation in a double quantum dot in the field of a micromagnet. *Phys. Rev. B* **90,** 235311 (2014).
37. Barthel, C., Reilly, D. J., Marcus, C. M., Hanson, M. P. & Gossard, A. C. Rapid Single-Shot Measurement of a Singlet-Triplet Qubit. *Phys. Rev. Lett.* **103,** 160503 (2009).
38. Potok, R. M. *et al.* Spin and Polarized Current from Coulomb Blockaded Quantum Dots. *Phys. Rev. Lett.* **91,** 016802 (2003).
39. Hanson, R. *et al.* Zeeman Energy and Spin Relaxation in a One-Electron Quantum Dot. *Phys. Rev. Lett.* **91,** 196802 (2003).
40. van Beveren, L. H. W. *et al.* Spin filling of a quantum dot derived from excited-state spectroscopy. *New J. Phys.* **7,** 182 (2005).
41. Borselli, M. G. *et al.* Pauli spin blockade in undoped Si/SiGe two-electron double quantum dots. *Appl. Phys. Lett.* **99,** 063109 (2011).
42. See, A. M. *et al.* Impact of Small-Angle Scattering on Ballistic Transport in Quantum Dots. *Phys. Rev. Lett.* **108,** 196807 (2012).
43. MacLeod, S. J. *et al.* Hybrid architecture for shallow accumulation mode AlGaAs/GaAs heterostructures with epitaxial gates. *Appl. Phys. Lett.* **106,** 012105 (2015).

Acknowledgements

We thank J. Beil, J. Medford, F. Kuemmeth, C. M. Marcus, D. J. Reilly, K. Ono, RIKEN CEMS Emergent Matter Science Research Support Team and Microwave Research Group in Caltech for fruitful discussions and technical supports. Part of this work is supported by the Grant-in-Aid for Scientific Research (No. 25800173, 26220710, 26709023, 26630151, 16H00817), CREST, JST, ImPACT Program of Council for Science, Technology and Innovation (Cabinet Office, Government of Japan), Strategic Information and Communications R&D Promotion Programme, RIKEN Incentive Research Project, Yazaki Memorial Foundation for Science and Technology Research Grant, Japan Prize Foundation Research Grant, Advanced Technology Institute Research Grant, the Murata Science Foundation Research Grant, Izumi Science and Technology Foundation Research Grant, TEPCO Memorial Foundation Research Grant, and IARPA project "Multi-Qubit Coherent Operations" through Copenhagen University. A.L. and A.D.W. acknowledge support of Mercur Pr-2013-0001, DFG-TRR160, BMBF - Q.com-H 16KIS0109, and the DFH/UFA CDFA-05-06.

Author Contributions

T.O., T.N., M.R.D., S.A., J.Y., K.T., G.A. and S.T. planned the project; T.O., T.N., M.R.D., S.A., A.L. and A.D.W. performed device fabrication; T.O., T.N., M.R.D., S.A., J.Y., K.T., G.A., T.I., R.S., A.N. and S.T. conducted experiments and data analysis; all authors discussed the results; T.O., T.N., M.R.D., S.A., J.Y., K.T., G.A. and S.T. wrote the manuscript.

Additional Information

Supplementary information accompanies this paper at http://www.nature.com/srep

Competing financial interests: The authors declare no competing financial interests.

How to cite this article: Otsuka, T. *et al.* Single-electron Spin Resonance in a Quadruple Quantum Dot. *Sci. Rep.* **6**, 31820; doi: 10.1038/srep31820 (2016).